

5.3 Charge Transfer Properties

We have seen that the final structure of the pentacene systems becomes more ordered and crystal-like as the quenching time is increased. It would be good now to see how this affects the charge transfer properties. A key quantity governing charge transfer rates is the ratio between electronic coupling and reorganisation energy, $\frac{H_{ab}}{\lambda}$. Seeing as we have a single molecule system, by plotting the electronic coupling we can get a qualitative view of the charge transfer dynamics and see which paths are the most likely within the structure.

5.3.1 Coupling Graphs

In figure 5.10 the graph of electronic couplings between molecules has been plotted for each of the quenched systems and a crystal system after a short equilibration run with MD. In this figure the centers of mass each molecule is represented by a small black dot and the calculated coupling value with a coloured line (red, green blue). That is, if 2 molecules have a non-negligible coupling between them they would be represented by 2 black dots with either a red, green or blue line connecting them. The couplings were calculated via the analytic overlap method⁴⁴ and a pertinent cluster of molecules was selected for each quench time. For the 0ns and 1ns quench times this was simply a slice 1 molecule thick in the z dimension, containing a few hundred molecules. For the 10ns and 100ns quenched structures a reasonable cluster of molecules was chosen after applying a density based clustering algorithm on the superstructure. For the crystal a plane from the crystal was chosen. All panes in figure 5.10 show the coupling of the selected system from an angle perpendicular to the plane of molecules.

We can see in the graph of the 0ns quenched structure there is very little order to the coupling network. Only very small fragments of high (red) coupling are formed and each one is connected via weak or medium coupling. We can define a 'high coupling fragment' as any set of molecules which can all be reached from any member of the set via an unbroken path of high coupling. The mean size of these high coupling fragments in the 0ns structure is 4.1 molecules and there are 503 of them. In this structure we would expect to see a localised polaron (over a ~ 3 molecules) and low mobilities due to the

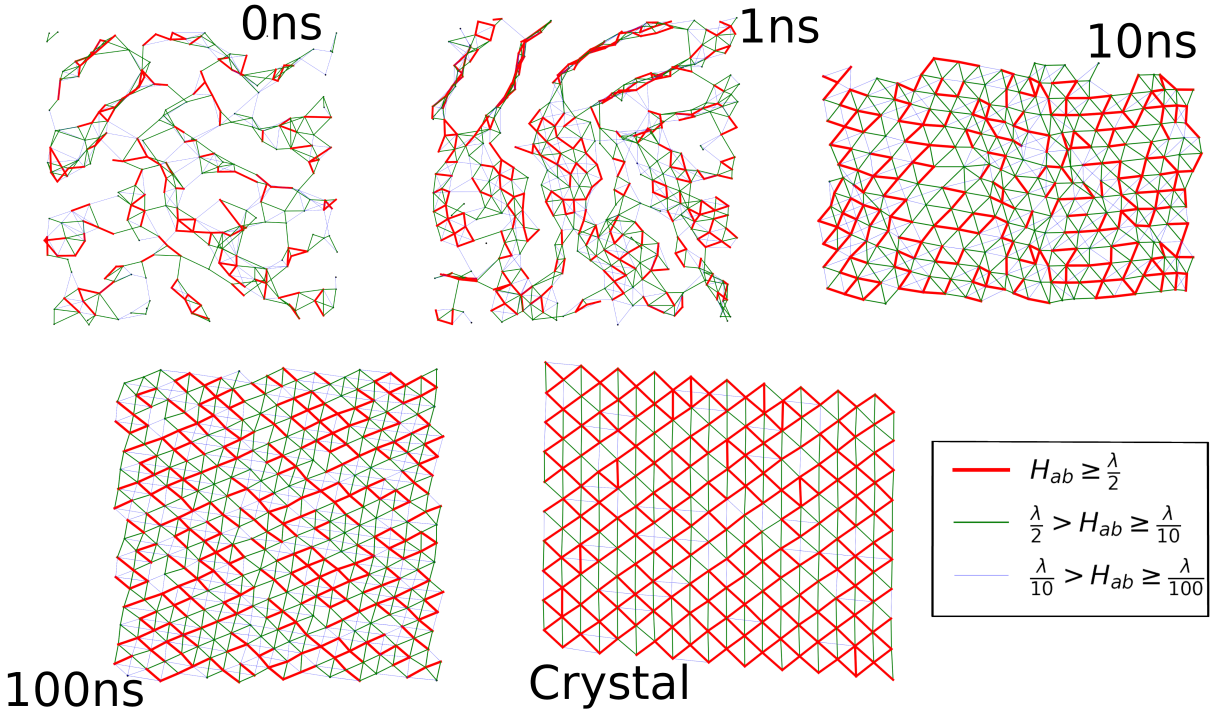


Figure 5.10: A representative network of electronic coupling that each quenched structure has formed. Each structure is labelled by the quench time (e.g. 0ns, 1ns, 10ns) or Crystal for a crystal after a short MD equilibration. Coupling strengths are categorised as high (red), medium (green) and low (blue). The definitions of the categories are given in the legend in the bottom right corner.

lack of conductive channels in the structure. The mean size of fragments increases and the number of fragments decreases as we increase the quenching time as shown in table 5.1.

Quench Time [ns]	Mean Fragment Size	Fragment Size Std Dev	Num Fragments
0	4.2	3.8	503
1	4.5	5.0	493
10	6.5	9.3	373
100	8.7	16.2	292

Table 5.1: The change in the number of high coupling fragments, and the mean and standard deviation of their size, found in each structure as the quenching time was varied.

We can see in table 5.1 that as the quenching time increases, the size of the highly coupled fragments (how many molecules are connected) increases and fewer of them are

formed. The standard deviation also increases showing in the 0ns quenched structure most fragments are very small but as we increase the quench time we still get smaller fragments but much larger ones can now form too. These larger fragments can act as regions of high conductivity allowing much larger mobilities to be achieved than in the quicker quenching times.

5.3.2 Hole Mobilities

To properly quantify the charge transfer dynamics the electron-hole mobility can be calculated on the output of a surface hopping simulation. A full discussion of the calculation of the electron mobility can be found here in Giannini, 19⁹. The mean squared displacement (MSD) of the charge carrier wavefunction was calculated and the gradient found by fitting a straight line to this. The gradient of the MSD, which is proportional to the Einstein diffusion coefficient D , was then used to calculate the mobility as in equation (5.2) below.

$$\mu_{ij} = \frac{eD_{ij}}{k_B T} \quad (5.2)$$

Where D_{ij} represents the Einstein diffusion coefficient, k_B is the Boltzmann constant, e the elementary charge and T is the temperature.

5.3.3 Simulation Set up

The surface hopping simulations require a swarm of hundreds of independent trajectories (~ 200), each with slightly different positions and velocities to fully sample phase space. The code currently does not support electrostatic interactions, so, in order to maintain the structure from the molecular dynamics simulations, center of mass restraints were used on each molecule. The restraint set up for 1 molecule is shown in figure 5.11. Here each of the 4 coloured zig-zag shapes show which atoms are restrained. These atoms were restrained about their

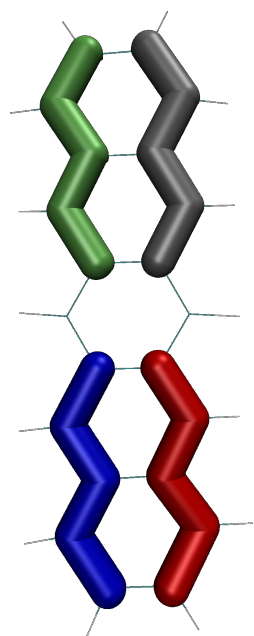


Figure 5.11: The restraint set up for 1 molecule. Each coloured zig-zag shows the atoms that are restrained.

center of mass. This configuration of restraints was used in order to stop rotations about the long axis for each molecule as this would allow molecules to form a face-to-face stacking giving rise to unphysically high couplings.

The restraints were tested ... Sam tested similar restraints

In order to obtain initial positions and velocities for the individual trajectories an MD equilibration was carried out using the restraint set up. This was carried out for 220ps using the NVE ensemble. The first 4ps were discarded and positions and velocities were then sampled every 1ps in order to get 216 trajectories. When these 216 trajectories were created, the Hamiltonian was calculated for each. This allowed an adiabatic state to be selected which, when transformed to the diabatic basis gave a population close to the center of the system and had an energy within 3KT of the ground state energy. An explanation of how this was done is given in appendix D. In short the method consisted of finding the adiabatic energy (eigenvalue) and diabatic populations (eigenvector) corresponding to adiabatic state n which yielded a state both close to the center and within approximately 3KT of the ground state energy. This was done to ensure a quick convergence of the mean squared displacement of the charge carrier. The surface hopping simulations were then carried out with initial positions and velocities coming from the NVE equilibration run and the initial wavefunction being selected as mentioned above. Other parameters were taken from previous surface hopping simulations carried out by other members of the group.

5.3.3.1 0ns and 1ns Systems

The region selected to run the surface hopping calculations on was important in order to get a fair representation of the mobilities achievable within each structure. In the 0ns and 1ns quenched structures 6 slices were selected from the final snapshot of the structure

5.3.4 Molecular Dynamics without Partial Charges

Appendix A

Tully Model Paramters

A.1 Model 1 -Single Avoided Crossing

	Quantity	Value	Unit
Hamiltonian Paramters:			
$H_{11}(\mathbf{R}) = A \tanh(B\mathbf{R})$	Initial Position	-20	a.u.
$H_{12}(\mathbf{R}) = Ce^{-D\mathbf{R}^2}$	Initial Velocities	15.0, 25.0	a.u.
$H_{21}(\mathbf{R}) = H_{12}(\mathbf{R})$	Initial Adiab Pop	ground state	-
$H_{22}(\mathbf{R}) = -H_{11}(\mathbf{R})$	Simulation Time	6000, 4000	a.u.
Where $A = 0.03$, $B = 0.4$, $C = 0.005$ and $D = 0.3$	$\sigma_v^{(I)}$	0.5	a.u.
	M (σ constant)	40	-
	$\Delta t_{\text{nuclear}}$	0.1	fs
	$\Delta t_{\text{electronic}}$	0.01	fs
	$\frac{\delta \mathbf{R}_{lk,v}^{(I)}}{\delta t}$ threshold	0.15	a.u.
	N_{rep}	200	-

A.2 Model 2 -Dual Avoided Crossing

	Quantity	Value	Unit
Hamiltonian Paramters:			
$H_{11}(\mathbf{R}) = 0$	Initial Position	-8	a.u.
$H_{12}(\mathbf{R}) = Ce^{-D\mathbf{R}^2}$	Initial Velocities	16.0, 30.0	a.u.
$H_{21}(\mathbf{R}) = H_{12}(\mathbf{R})$	Initial Adiab Pop	ground state	-
$H_{22}(\mathbf{R}) = -Ae^{-B\mathbf{R}^2} + E$	Simulation Time	2500, 1500	a.u.
Where A = 0.1, B = 0.28, C = 0.015, D = 0.06 and E = 0.05	$\sigma_v^{(I)}$	0.5	a.u.
	M (σ constant)	40	-
	$\Delta t_{\text{nuclear}}$	0.1	fs
	$\Delta t_{\text{electronic}}$	0.01	fs
	$\frac{\delta \mathbf{R}_{ik,v}^{(I)}}{\delta t}$ threshold	0.15	a.u.
	N_{rep}	200	-

A.3 Model 3 -Extended Coupling

	Quantity	Value	Unit
Hamiltonian Paramters:			
$H_{11}(\mathbf{R}) = A$	Initial Position	-15	a.u.
$H_{12}(\mathbf{R}) = \begin{cases} Be^{C\mathbf{R}}, & R \leq 0 \\ B(2 - e^{-C\mathbf{R}}), & R > 0 \end{cases}$	Initial Velocities	10, 30	a.u.
$H_{21}(\mathbf{R}) = H_{12}(\mathbf{R})$	Initial Adiab Pop	ground state	-
$H_{22}(\mathbf{R}) = -H_{11}(\mathbf{R})$	Simulation Time	5000, 1500	a.u.
Where A = 6×10^{-4} , B = 0.1 and C = 0.9	$\sigma_v^{(I)}$	0.5	a.u.
	M (σ constant)	40	-
	$\Delta t_{\text{nuclear}}$	0.1	fs
	$\Delta t_{\text{electronic}}$	0.01	fs
	$\frac{\delta \mathbf{R}_{ik,v}^{(I)}}{\delta t}$ threshold	0.15	a.u.
	N_{rep}	200	-

A.4 Model 4 -Dual Arch

Hamiltonian Paramters:

$$H_{11}(\mathbf{R}) = A$$

$$H_{12}(\mathbf{R}) = \begin{cases} B \left[-e^{C(\mathbf{R}-D)} + e^{C(\mathbf{R}+D)} \right] & R \leq -D \\ B \left[e^{-C(\mathbf{R}-D)} - e^{-C(\mathbf{R}+D)} \right] & R \geq D \\ B \left[2 - e^{C(\mathbf{R}-D)} - e^{-C(\mathbf{R}+D)} \right] & -D < R < D \end{cases}$$

$$H_{21}(\mathbf{R}) = H_{12}(\mathbf{R})$$

$$H_{22}(\mathbf{R}) = -H_{11}(\mathbf{R})$$

Where $A = 6 \times 10^{-4}$, $B = 0.1$ and $C = 0.9$

Quantity	Value	Unit
Initial Position	-20	a.u.
Initial Velocities	10, 40	a.u.
Initial Adiab Pop	ground state	-
Simulation Time	6000, 2000	a.u.
$\sigma_v^{(I)}$	0.5	a.u.
M (σ constant)	40	-
$\Delta t_{\text{nuclear}}$	0.1	fs
$\Delta t_{\text{electonic}}$	0.01	fs
$\frac{\delta \mathbf{R}_{lk,v}^{(I)}}{\delta t}$ threshold	0.15	a.u.
N_{rep}	200	-

Appendix B

Wigner Distribution Derivation

The nuclear wavepacket (at time 0) is given by:

$$\chi(R) = \frac{1}{(\pi\mu^2)^{\frac{1}{4}}} e^{-\frac{(R-R_0)^2}{2\mu^2} + ik_0(R-R_0)} \quad (\text{B.1})$$

The Wigner quasiprobability function for momentum and position (p, R) is given by:

$$W(p, R) = \frac{1}{\pi\hbar} \int_{-\infty}^{\infty} \chi^*(R+y)\chi(R-y)e^{\frac{2ipy}{\hbar}} dy \quad (\text{B.2})$$

However, both Ehrenfest and CTMQC require atomic positions as input so we must extract the position and velocity probability densities from this. We get these from the marginal integrals of the Wigner distribution i.e.

$$|f(R)|^2 = \int_{-\infty}^{\infty} W(R, p) dp \quad (\text{B.3})$$

$$|f(p)|^2 = \int_{-\infty}^{\infty} W(R, p) dR \quad (\text{B.4})$$

In order to calculate these marginal integrals we must first crunch through the maths of equation (B.2). Substituting eq (B.1) into (B.2):

$$W(p, R) = \frac{1}{\pi\hbar} \int_{-\infty}^{\infty} \frac{1}{\mu\sqrt{\pi}} e^{-\frac{(R+y-R_0)^2}{2\mu^2} - 2ik_0y - \frac{(R-y-R_0)^2}{2\mu^2}} e^{\frac{2ipy}{\hbar}} dy \quad (\text{B.5})$$

Simplifying the 2 quadratic equations (equation (B.5)) we get:

$$W(p, R) = \frac{1}{\pi \hbar} \int_{-\infty}^{\infty} \frac{1}{\mu \sqrt{\pi}} e^{-\mu^{-2}(y^2 - 2ik_0 y \mu^2 + (R-R_0)^2)} e^{\frac{2ipy}{\hbar}} dy \quad (\text{B.6})$$

We can now take the expressions not dependant on y outside of the integral and combine the exponents.

$$W(p, R) = \frac{1}{\pi \sqrt{\pi} \mu \hbar} e^{-\frac{(R-R_0)^2}{\mu^2}} \int_{-\infty}^{\infty} e^{-\frac{y^2 + 2iy\mu^2(\frac{p}{\hbar} - k_0)}{\mu^2}} dy \quad (\text{B.7})$$

Integrating we get:

$$\int e^{-\frac{y^2 + 2iy\mu^2(\frac{p}{\hbar} - k_0)}{\mu^2}} dy = \frac{\sqrt{\pi} \mu}{2} e^{-\frac{\mu^2}{\hbar^2}(p - \hbar k_0)^2} \operatorname{erf} \left[\frac{y}{\mu} + i \left(\frac{p\mu}{\hbar} - \mu k_0 \right) \right] \quad (\text{B.8})$$

Applying limits we get:

$$\int_{-\infty}^{\infty} e^{-\frac{y^2 + 2iy\mu^2(\frac{p}{\hbar} - k_0)}{\mu^2}} dy = \sqrt{\pi} \mu e^{-\frac{\mu^2}{\hbar^2}(p - \hbar k_0)^2} \quad (\text{B.9})$$

Substituting this back into the Wigner distribution (equation (B.2)) we finally get:

$$W(p, R) = \frac{1}{\pi \hbar} e^{-\frac{(R-R_0)^2}{\mu^2}} e^{-\frac{(p - \hbar k_0)^2}{\hbar^2/\mu^2}} \quad (\text{B.10})$$

Taking the marginal integrals we get the position and velocity probability distributions:

$$|f(R)|^2 = \frac{2}{\mu \sqrt{\pi}} e^{-\frac{(R-R_0)^2}{\mu^2}} \quad (\text{B.11})$$

$$|f(p)|^2 = \frac{2}{\frac{\hbar}{\mu} \sqrt{\pi}} e^{-\frac{\mu^2}{\hbar^2}(p - \hbar k_0)^2} \quad (\text{B.12})$$

The above distributions are randomly sampled to get initial atomic velocities and positions for each simulation.

Appendix C

Norm Conservation in CTMQC and Ehrenfest

A statement of the conservation of the norm is given below in equation (C.1)

$$\frac{d}{dt} \sum_l |C_l(t)|^2 = \sum_l C_l^*(t) \frac{dC_l(t)}{dt} + \frac{dC_l^*(t)}{dt} C_l(t) = 0 \quad (\text{C.1})$$

Because the adiabatic populations are real we can remove any imaginary parts.

$$\frac{d}{dt} \sum_l |C_l(t)|^2 = 2\mathbb{R} \left[C_l^*(t) \frac{dC_l(t)}{dt} \right] \quad (\text{C.2})$$

Substituting the equation for the evolution of the adiabatic coefficients (and removing the purely imaginary term into (C.2) we get equation (C.4)

$$\begin{aligned} \frac{d}{dt} \sum_l |C_l(t)|^2 &= 2 \sum_l \mathbb{R} \left[\frac{-i}{\hbar} \cancel{\epsilon_{BO}^l} C_l(t)^* \cancel{C_l(t)} - \sum_k C_l(t)^* C_k(t) d_{lk}^{ad} - (K^{sum} - K_l^{ad}) C_l(t)^* C_l(t) \right] \\ &\quad (\text{C.3}) \end{aligned}$$

$$= -2 \sum_l \mathbb{R} \left[\sum_k C_l(t)^* C_k(t) d_{lk}^{ad} - (K^{sum} - K_l^{ad}) C_l(t)^* C_l(t) \right] \quad (\text{C.4})$$

Where:

$$K^{sum} = \sum_{v=1}^{N_n} \sum_k \frac{\mathcal{Q}_{lk,v}(t)}{\hbar M_v} \cdot |C_k(t)|^2 \mathbf{f}_{k,v}(t) \quad (\text{C.5})$$

$$K_l^{ad} = \sum_{v=1}^{N_n} \sum_k \frac{\mathcal{Q}_{lk,v}(t)}{\hbar M_v} \cdot \mathbf{f}_{l,v}(t) \quad (\text{C.6})$$

The NACE term evaluates to 0 due to the anti-symmetry of the NACE giving us equation (C.8).

So far, we have proved that the norm should be conserved here for all terms apart from the quantum momentum terms i.e. Ehrenfest.

$$\frac{d}{dt} \sum_l |C_l(t)|^2 = 2 \sum_l \mathbb{R} \left[(K^{sum} - K_l^{ad}) C_l(t)^* C_l(t) \right] \quad (\text{C.7})$$

$$= 2 \left[K^{sum} - \sum_l K_l^{ad} |C_l(t)|^2 \right] \quad (\text{C.8})$$

However, $K^{sum} \equiv \sum_l K_l^{ad} |C_l|^2$, therefore the norm should be conserved when summed over trajectories. This statement doesn't apply to individual trajectories though, and the norm may or may not be conserved for each of them. This is because they are coupled via the quantum momentum and population may transfer between trajectories.

Appendix D

Adiabatic State Initialisation

By diagonalising the Hamiltonian we get the adiabatic energies (eigenvalues) for each state and transformation matrix (eigenvectors) to calculate diabatic states \mathbb{U} . We can calculate diabatic coefficients corresponding to each adiabatic state via equation (D.1) below.

$$\mathbb{U}\mathbf{C}_n = \mathbf{u}_n \quad (\text{D.1})$$

Where \mathbb{U} is the transformation matrix of size $(N_{\text{mol}}, N_{\text{mol}})$, \mathbf{C} is a complex vector of size N_{mol} containing coefficients for adiabatic state n and \mathbf{u} is a complex vector of size N_{mol} containing coefficients for diabatic state n .

Seeing as we would like to find the diabatic population corresponding to each adiabatic state we localise coefficients on each pure adiabatic state and carry out the transformation e.g: $C_i = (1+0i, 0+0i, 0+0i, \dots)$ when we want to find the diabatic coefficient corresponding to state 1 and $C_i = (0+0i, 1+0i, 0+0i, \dots)$ when we want to find the diabatic coefficient corresponding to state 2 etc.. Therefore, the column, n , of the transformation matrix, \mathbb{U} , gives the diabatic coefficients corresponding to adiabatic state, n , as shown below in equation (D.2)

$$U_{in} = u_i \quad (\text{D.2})$$

Where n is the adiabatic state index and i is the diabatic (molecular) state index.

Once we have the diabatic state corresponding to each adiabatic state, and the en-

ergy of that adiabatic state, we can find which state best fulfills the requirements of being close to the center of the system and being within $3KT$ of the ground state. In order to do this, we can loop over each adiabatic state in increasing order of energy. The center of the system is calculated and the population weighted average center of mass, \mathbf{R}_n of the diabatic coefficients corresponding to adiabatic state n is calculated as in equation (D.3).

$$\mathbf{R}_n = \sum_i |u_i|^2 \mathbf{R}_{COM,i} \quad (\text{D.3})$$

The Euclidean distance between the center of the system and $\mathbf{R}_{COM,i}$ is calculated and if this distance is below some threshold value then we initialise the surface hopping trajectory on that adiabatic state. If we do not find any states within $3KT$ of the ground state and within an acceptable radius of the center we start again this time increasing the maximum allowed distance from the center. If this maximum allowed distance is increased such that we reach another threshold distance the energy threshold is increased this time until a state is found that is close enough to the center. In this way we find an adiabatic state, which when transformed, gives a diabatic population close to center of the system and near the ground state energy.

Appendix E

Colophon

This is a description of the tools you used to make your thesis. It helps people make future documents, reminds you, and looks good.

(example) This document was set in the Times Roman typeface using L^AT_EX (specifically LuaTeX) and BibTeX, composed with Vim Used Archer, Kathleen etc...

Bibliography

- [1] C. K. Chiang, C. R. Fincher, Y. W. Park, A. J. Heeger, H. Shirakawa, E. J. Louis, S. C. Gau, and Alan G. MacDiarmid. Electrical Conductivity in Doped Polyacetylene. *Physical Review Letters*, 39(17):1098–1101, October 1977.
- [2] Hideki Shirakawa, Edwin J. Louis, Alan G. MacDiarmid, Chwan K. Chiang, and Alan J. Heeger. Synthesis of electrically conducting organic polymers: halogen derivatives of polyacetylene, $(CH)_x$. *J. Chem. Soc., Chem. Commun.*, 0(16):578–580, Jan 1977.
- [3] Bernard Kippelen and Jean-Luc Brédas. Organic photovoltaics. *Energy Environ. Sci.*, 2(3):251–261, 2009.
- [4] M. J. Małachowski and J. Żmija. Organic field-effect transistors. *Opto-Electron. Rev.*, 18(2):121–136, Jun 2010.
- [5] N. Thejo Kalyani and S. J. Dhoble. Organic light emitting diodes: Energy saving lighting technology—A review. *Renewable Sustainable Energy Rev.*, 16(5):2696–2723, Jun 2012.
- [6] Sebastian Reineke, Frank Lindner, Gregor Schwartz, Nico Seidler, Karsten Walzer, Björn Lüssem, and Karl Leo. White organic light-emitting diodes with fluorescent tube efficiency. *Nature*, 459(7244):234, May 2009.
- [7] Kazuki Kato, Toshihiko Iwasaki, and Takatoshi Tsujimura. Over 130 lm/w all-phosphorescent white oleds for next-generation lighting. *Journal of Photopolymer Science and Technology*, 28:335–340, 10 2015.

- [8] Veaceslav Coropceanu, Jérôme Cornil, Demetrio A. da Silva Filho, Yoann Olivier, Robert Silbey, and Jean-Luc Brédas. Charge Transport in Organic Semiconductors. *Chemical Reviews*, 107(4):926–952, April 2007.
- [9] Samuele Giannini, Antoine Carof, Matthew Ellis, Hui Yang, Orestis George Ziosgos, Soumya Ghosh, and Jochen Blumberger. Quantum localization and delocalization of charge carriers in organic semiconducting crystals. *Nature Communications*, 10(1):3843, Aug 2019.
- [10] Alessandro Troisi. Charge transport in high mobility molecular semiconductors: classical models and new theories. *Chem. Soc. Rev.*, 40:2347–2358, 2011.
- [11] Simone Fratini, Didier Mayou, and Sergio Ciuchi. The transient localization scenario for charge transport in crystalline organic materials. *Advanced Functional Materials*, 26(14):2292–2315, 2016.
- [12] I. Yavuz. Dichotomy between the band and hopping transport in organic crystals: insights from experiments. *Physical Chemistry Chemical Physics*, 19(38):25819–25828, 2017.
- [13] J. S. Brown and S. E. Shaheen. Introducing correlations into carrier transport simulations of disordered materials through seeded nucleation: impact on density of states, carrier mobility, and carrier statistics. *J. Phys.: Condens. Matter*, 30(13):135702, Mar 2018.
- [14] Tino Zimmerling and Bertram Batlogg. Improving charge injection in high-mobility rubrene crystals: From contact-limited to channel-dominated transistors. *Journal of Applied Physics*, 115(16):164511, 2014.
- [15] V. Podzorov, E. Menard, A. Borissov, V. Kiryukhin, J. A. Rogers, and M. E. Gershenson. Intrinsic charge transport on the surface of organic semiconductors. *Phys. Rev. Lett.*, 93:086602, Aug 2004.
- [16] Samuele Giannini, Antoine Carof, and Jochen Blumberger. Crossover from Hopping to Band-Like Charge Transport in an Organic Semiconductor Model: Atomistic

- Nonadiabatic Molecular Dynamics Simulation. *The Journal of Physical Chemistry Letters*, 9(11):3116–3123, June 2018.
- [17] Harald Oberhofer, Karsten Reuter, and Jochen Blumberger. Charge Transport in Molecular Materials: An Assessment of Computational Methods. *Chemical Reviews*, 117(15):10319–10357, August 2017.
- [18] John C. Tully. Nonadiabatic Dynamics. pages 34–71.
- [19] Simone Pisana, Michele Lazzeri, Cinzia Casiraghi, Kostya S. Novoselov, A. K. Geim, Andrea C. Ferrari, and Francesco Mauri. Breakdown of the adiabatic Born–Oppenheimer approximation in graphene. *Nat. Mater.*, 6(3):198, Feb 2007.
- [20] M. Born and R. Oppenheimer. Zur Quantentheorie der Molekeln. *Ann. Phys.*, 389(20):457–484, Jan 1927.
- [21] Sharon Hammes-Schiffer. Theoretical Perspectives on Proton-Coupled Electron Transfer Reactions. *Acc. Chem. Res.*, 34(4):273–281, Apr 2001.
- [22] Sharon Hammes-Schiffer and John C. Tully. Proton transfer in solution: Molecular dynamics with quantum transitions. *J. Chem. Phys.*, 101(6):4657–4667, Sep 1994.
- [23] My Hang V. Huynh and Thomas J. Meyer. Proton-coupled electron transfer. *Chemical Reviews*, 107(11):5004–5064, Nov 2007.
- [24] John C. Tully. Nonadiabatic molecular dynamics. *International Journal of Quantum Chemistry*, 40(S25):299–309, 1991.
- [25] Raymond Kapral and Giovanni Ciccotti. Mixed quantum-classical dynamics. *J. Chem. Phys.*, 110(18):8919–8929, May 1999.
- [26] Todd J. Martínez*. Insights for Light-Driven Molecular Devices from Ab Initio Multiple Spawning Excited-State Dynamics of Organic and Biological Chromophores. American Chemical Society, Oct 2005.

- [27] Guillermo Albareda, Heiko Appel, Ignacio Franco, Ali Abedi, and Angel Rubio. Correlated Electron-Nuclear Dynamics with Conditional Wave Functions. *Phys. Rev. Lett.*, 113(8):083003, Aug 2014.
- [28] John C. Tully. Molecular dynamics with electronic transitions. *J. Chem. Phys.*, 93(2):1061–1071, Jul 1990.
- [29] R. L et al Whetten. Molecular dynamics beyond the adiabatic approximation: New experiments and theory. *Ann. Rev. Phys. Chem.*, 36:277–320.
- [30] Neil Shenvi, Joseph E. Subotnik, and Weitao Yang. Simultaneous-trajectory surface hopping: A parameter-free algorithm for implementing decoherence in nonadiabatic dynamics. *J. Chem. Phys.*, 134(14):144102, Apr 2011.
- [31] D. F. Coker and L. Xiao. Methods for molecular dynamics with nonadiabatic transitions. *J. Chem. Phys.*, 102(1):496–510, Jan 1995.
- [32] Joseph E. Subotnik, Amber Jain, Brian Landry, Andrew Petit, Wenjun Ouyang, and Nicole Bellonzi. Understanding the surface hopping view of electronic transitions and decoherence. *Annual Review of Physical Chemistry*, 67(1):387–417, 2016. PMID: 27215818.
- [33] Giovanni Granucci, Maurizio Persico, and Alberto Zoccante. Including quantum decoherence in surface hopping. *The Journal of Chemical Physics*, 133(13):134111, 2010.
- [34] Heather M. Jaeger, Sean Fischer, and Oleg V. Prezhdo. Decoherence-induced surface hopping. *The Journal of Chemical Physics*, 137(22):22A545, 2012.
- [35] Amber Jain, Ethan Alguire, and Joseph E. Subotnik. An efficient, augmented surface hopping algorithm that includes decoherence for use in large-scale simulations. *Journal of Chemical Theory and Computation*, 12(11):5256–5268, Nov 2016.
- [36] Joseph E. Subotnik and Neil Shenvi. A new approach to decoherence and momentum rescaling in the surface hopping algorithm. *The Journal of Chemical Physics*, 134(2):024105, 2011.

- [37] Xiaosong Li, John C. Tully, H. Bernhard Schlegel, and Michael J. Frisch. Ab initio Ehrenfest dynamics. *J. Chem. Phys.*, 123(8):084106, Aug 2005.
- [38] Kenichiro Saita and Dmitrii V. Shalashilin. On-the-fly ab initio molecular dynamics with multiconfigurational Ehrenfest method. *J. Chem. Phys.*, 137(22):22A506, Dec 2012.
- [39] Daniela Kohen, Frank H. Stillinger, and John C. Tully. Model studies of nonadiabatic dynamics. *J. Chem. Phys.*, 109(12):4713–4725, Sep 1998.
- [40] John C. Tully. Perspective: Nonadiabatic dynamics theory. *The Journal of Chemical Physics*, 137(22):22A301, December 2012.
- [41] Priya V. Parandekar and John C. Tully. Detailed Balance in Ehrenfest Mixed Quantum-Classical Dynamics. *Journal of Chemical Theory and Computation*, 2(2):229–235, March 2006.
- [42] John C. Tully. Molecular dynamics with electronic transitions. *The Journal of Chemical Physics*, 93(2):1061–1071, July 1990.
- [43] Graeme H. Gossel, Federica Agostini, and Neepa T. Maitra. Coupled-Trajectory Mixed Quantum-Classical Algorithm: A Deconstruction. *Journal of Chemical Theory and Computation*, August 2018.
- [44] Fruzsina Gajdos, Siim Valner, Felix Hoffmann, Jacob Spencer, Marian Breuer, Adam Kubas, Michel Dupuis, and Jochen Blumberger. Ultrafast Estimation of Electronic Couplings for Electron Transfer between -Conjugated Organic Molecules. *Journal of Chemical Theory and Computation*, 10(10):4653–4660, October 2014.
- [45] J. VandeVondele, J; Hutter. Gaussian basis sets for accurate calculations on molecular systems in gas and condensed phases. *The Journal of Chemical Physics*, 127(11).
- [46] J. Spencer, F. Gajdos, and J. Blumberger. FOB-SH: Fragment orbital-based surface hopping for charge carrier transport in organic and biological molecules and materials. *The Journal of Chemical Physics*, 145(6):064102, August 2016.

- [47] Antoine Carof, Samuele Giannini, and Jochen Blumberger. Detailed balance, internal consistency, and energy conservation in fragment orbital-based surface hopping. *The Journal of Chemical Physics*, 147(21):214113, December 2017.
- [48] Biswajit Ray, Aditya G. Baradwaj, Bryan W. Boudouris, and Muhammad A. Alam. Defect characterization in organic semiconductors by forward bias capacitance–voltage (fb-cv) analysis. *The Journal of Physical Chemistry C*, 118(31):17461–17466, Aug 2014.
- [49] W. S. Hu, Y. T. Tao, Y. J. Hsu, D. H. Wei, and Y. S. Wu. Molecular orientation of evaporated pentacene films on gold: alignment effect of self-assembled monolayer. *Langmuir*, 21(6):2260–2266, Mar 2005.
- [50] Tatsuo Hasegawa and Jun Takeya. Organic field-effect transistors using single crystals. *Science and Technology of Advanced Materials*, 10(2):024314, 2009.
- [51] John E. Anthony, James S. Brooks, David L. Eaton, and Sean R. Parkin. Functionalized pentacene: improved electronic properties from control of solid-state order. *Journal of the American Chemical Society*, 123(38):9482–9483, Sep 2001.
- [52] John E. Anthony, David L. Eaton, and Sean R. Parkin. A road map to stable, soluble, easily crystallized pentacene derivatives. *Organic Letters*, 4(1):15–18, Jan 2002.
- [53] A. D’Angelo, B. Edgar, A. P. Hurt, and M. D. Antonijević. Physico-chemical characterisation of three-component co-amorphous systems generated by a melt-quench method. *Journal of Thermal Analysis and Calorimetry*, 134(1):381–390, Oct 2018.
- [54] Wanderlā L. Scopel, Antônio J. R. da Silva, and A. Fazzio. Amorphous hfo_2 and $\text{hf}_{1-x}\text{si}_x\text{O}$ via a melt-and-quench scheme using ab initio molecular dynamics. *Phys. Rev. B*, 77:172101, May 2008.
- [55] Seth S. Berbano, Inseok Seo, Christian M. Bischoff, Katherine E. Schuller, and Steve W. Martin. Formation and structure of $\text{na}_2\text{s}+\text{p}_2\text{s}_5$ amorphous materials prepared by melt-quenching and mechanical milling. *Journal of Non-Crystalline Solids*, 358(1):93 – 98, 2012.

- [56] Pranav Karmwar, Kirsten Graeser, Keith C. Gordon, Clare J. Strachan, and Thomas Rades. Investigation of properties and recrystallisation behaviour of amorphous indomethacin samples prepared by different methods. *International Journal of Pharmaceutics*, 417(1):94 – 100, 2011. Advanced characterization techniques.
- [57] Min-Jin Ko, Joel Plawsky, and Meyer Birnboim. Fabrication of cds/ag hybrid quantum dot composites using a melt/quench method. *Journal of Non-Crystalline Solids*, 203:211 – 216, 1996. Optical and Electrical Propertias of Glasses.
- [58] Steve Plimpton. Fast parallel algorithms for short-range molecular dynamics. *Journal of Computational Physics*, 117(1):1 – 19, 1995.
- [59] Steve Plimpton. Lammps software. <http://lammps.sandia.gov>, 1995. [Online; accessed 21-Jan-2021].
- [60] Steve Plimpton, Roy Pollock, and Mark Stevens. Particle-mesh ewald and rrespa for parallel molecular dynamics simulations. In In Proceedings of the Eighth SIAM Conference on Parallel Processing for Scientific Computing, 1997.
- [61] Christopher I. Bayly, Piotr Cieplak, Wendy Cornell, and Peter A. Kollman. A well-behaved electrostatic potential based method using charge restraints for deriving atomic charges: the resp model. *The Journal of Physical Chemistry*, 97(40):10269–10280, Oct 1993.
- [62] M. J. Frisch, G. W. Trucks, H. B. Schlegel, G. E. Scuseria, M. A. Robb, J. R. Cheeseman, G. Scalmani, V. Barone, G. A. Petersson, H. Nakatsuji, X. Li, M. Caricato, A. V. Marenich, J. Bloino, B. G. Janesko, R. Gomperts, B. Mennucci, H. P. Hratchian, J. V. Ortiz, A. F. Izmaylov, J. L. Sonnenberg, D. Williams-Young, F. Ding, F. Lipparini, F. Egidi, J. Goings, B. Peng, A. Petrone, T. Henderson, D. Ranasinghe, V. G. Zakrzewski, J. Gao, N. Rega, G. Zheng, W. Liang, M. Hada, M. Ehara, K. Toyota, R. Fukuda, J. Hasegawa, M. Ishida, T. Nakajima, Y. Honda, O. Kitao, H. Nakai, T. Vreven, K. Throssell, J. A. Montgomery, Jr., J. E. Peralta, F. Ogliaro, M. J. Bearpark, J. J. Heyd, E. N. Brothers, K. N. Kudin, V. N. Staroverov, T. A. Keith, R. Kobayashi, J. Normand, K. Raghavachari, A. P. Rendell,

- J. C. Burant, S. S. Iyengar, J. Tomasi, M. Cossi, J. M. Millam, M. Klene, C. Adamo, R. Cammi, J. W. Ochterski, R. L. Martin, K. Morokuma, O. Farkas, J. B. Foresman, and D. J. Fox. Gaussian[®]16 Revision C.01, 2016. Gaussian Inc. Wallingford CT.
- [63] Junmei Wang, Romain M. Wolf, James W. Caldwell, Peter A. Kollman, and David A. Case. Development and testing of a general amber force field. *Journal of Computational Chemistry*, 25(9):1157–1174, 2004.
- [64] Makoto Yoneya, Masahiro Kawasaki, and Masahiko Ando. Molecular dynamics simulations of pentacene thin films: The effect of surface on polymorph selection. *J. Mater. Chem.*, 20:10397–10402, 2010.
- [65] Makoto Yoneya, Masahiro Kawasaki, and Masahiko Ando. Are pentacene monolayer and thin-film polymorphs really substrate-induced? a molecular dynamics simulation study. *The Journal of Physical Chemistry C*, 116(1):791–795, Jan 2012.
- [66] Makoto Yoneya. Simulation of crystallization of pentacene and its derivatives from solution. *The Journal of Physical Chemistry C*, Jan 2021.
- [67] Ryan A. Miller, Amanda Larson, and Karsten Pohl. Novel surface diffusion characteristics for a robust pentacene derivative on au(111) surfaces. *Chemical Physics Letters*, 678:28 – 34, 2017.
- [68] Dong Wang, Ling Tang, Mengqiu Long, and Zhigang Shuai. Anisotropic thermal transport in organic molecular crystals from nonequilibrium molecular dynamics simulations. *The Journal of Physical Chemistry C*, 115(13):5940–5946, Apr 2011.
- [69] Florian Steiner, Carl Poelking, Dorota Niedzialek, Denis Andrienko, and Jenny Nelson. Influence of orientation mismatch on charge transport across grain boundaries in tri-isopropylsilyl ethynyl (tips) pentacene thin films. *Phys. Chem. Chem. Phys.*, 19:10854–10862, 2017.
- [70] Ida Bagus Hendra Prastiawan, Jingxiang Xu, Yusuke Ootani, Yuji Higuchi, Nobuki Ozawa, Shingo Maruyama, Yuji Matsumoto, and Momoji Kubo. Molecular interac-

- tions between pentacene and imidazolium ionic liquids: A molecular dynamics study. *Chemistry Letters*, 47(9):1154–1157, 2018.
- [71] William Humphrey, Andrew Dalke, and Klaus Schulten. VMD – Visual Molecular Dynamics. *Journal of Molecular Graphics*, 14:33–38, 1996.
- [72] John Stone. An Efficient Library for Parallel Ray Tracing and Animation. Master’s thesis, Computer Science Department, University of Missouri-Rolla, April 1998.
- [73] EPA DSSTox. Epa dsstox. <https://comptox.epa.gov/dashboard/DTXSID7059648>, 2021. [Online; accessed 25-Jan-2021].
- [74] Stefan Schiefer, Martin Huth, Alexander Dobrinevski, and Bert Nickel. Determination of the crystal structure of substrate-induced pentacene polymorphs in fiber structured thin films. *Journal of the American Chemical Society*, 129(34):10316–10317, Aug 2007.